Effect of Metabolic Inhibition on Couplon Behavior in Rabbit Ventricular Myocytes

Chana Chantawansri,* Nhi Huynh,* Jun Yamanaka,* Alan Garfinkel,* Scott T. Lamp,* Masashi Inoue,† John H. B. Bridge,† and Joshua I. Goldhaber*

*Division of Cardiology, Cardiovascular Research Laboratories, David Geffen School of Medicine at UCLA, Los Angeles, California; and †Nora Eccles Harrison Cardiovascular Research and Training Institute, University of Utah, Salt Lake City, Utah

ABSTRACT We investigated the effect of combined inhibition of oxidative and glycolytic metabolism on L-type Ca^{2+} channels (LCCs) and Ca^{2+} spikes in isolated patch-clamped rabbit ventricular myocytes. Metabolic inhibition (MI) reduced LCC open probability, increased null probability, increased first latency, and decreased open time but left conductance unchanged. These results explain the reduction in macroscopic Ca^{2+} current observed during MI. MI also produced a gradual reduction in action potential duration at 90% repolarization (APD_{90}), a clear decline in spike probability, and an increase in spike latency and variance. These effects are consistent with the changes we observed in LCC activity. MI had no effect on the amplitude or time to peak of Ca^{2+} spikes until APD_{90} reached 10% of control, suggesting preserved sarcoplasmic reticulum Ca^{2+} stores and ryanodine receptor (RyR) conductance in those couplons that remained functioning. Ca^{2+} spikes disappeared completely when APD_{90} reached $<2\%$ of control, although in two cells, spikes were reactivated in a highly synchronized fashion by very short action potentials. This reactivation is probably due to the increased driving force for Ca^{2+} entry through a reduced number of LCCs that remain open during early repolarization. The enlarged single channel flux produced by rapid repolarization is apparently sufficient to trigger RyRs whose Ca^{2+} sensitivity is likely reduced by MI. We suggest that loss of coupling fidelity during MI is explained by loss of LCC activity (possibly mediated by Ca^{2+}-calmodulin kinase II activity). In addition, the results are consistent with loss of RyR activity, which can be mitigated under conditions likely to enlarge the trigger.

INTRODUCTION

Metabolic stress, a prominent feature of both cardiac ischemia and systolic heart failure, produces dramatic abnormalities in excitation-contraction (EC) coupling that contribute to contractile dysfunction (1,2). In voltage-clamped isolated ventricular myocytes, we have demonstrated that combined inhibition of oxidative and glycolytic metabolism with carbonyl cyanide-*p*-trifluoromethoxyphenylhydrazone (FCCP) and 2-deoxyglucose (2-DG) reduces the amplitude of L-type Ca^{2+} current (I_{Ca}), the Ca^{2+} transient, and EC coupling gain (defined as the ratio of Ca^{2+} release flux to I_{Ca}) (2). The reduction in gain is apparently due to the fractionation of the Ca^{2+} release pattern and loss of Ca^{2+} release sites, i.e., couplons (3,4) despite an intact sarcoplasmic reticulum (SR) Ca^{2+} load (2). Action potential duration (APD) shortening is another consequence of ischemia, hypoxia, and metabolic inhibition (MI), which is caused by a reduction in I_{Ca} and activation of I_{KATP}, the ATP-sensitive K^+ current (1). Ultimately, action potential (AP) failure results in electrical silence and thus complete contractile failure. It remains unclear whether Ca^{2+} release fails because of defective triggering by I_{Ca}, defective release of Ca^{2+} by ryanodine receptors (RyR), or a combination of both. However, in the extreme of electrical silence, failure of the trigger is a sufficient condition for failure of EC coupling.

Macroscopic Ca^{2+} current, and hence the trigger for Ca^{2+} release, could fail during MI for a number of reasons. First it is possible that the magnitude of unitary currents through L-type Ca^{2+} channels (LCCs) is reduced (i.e., the conductance of the channel could decline) during MI, which would reduce coupling fidelity (5). Other possible changes in LCC characteristics include: a decline in open probability, increases in null probability, changes in the distribution of first latencies, and finally, changes in the distribution of LCC open times. Currently, nothing is known of the behavior of LCCs during MI.

Besides the loss of I_{Ca}, and hence trigger, RyRs themselves are at risk during MI (1,2,6). Changes in pH, increases in Mg^{2+}, and declines in ATP could all contribute to loss of RyR function and hence, couplon activity. This could occur before the loss of trigger and might to some extent be reversible by enlarged triggers (7).

Here we have, for the first time, studied single LCC activity, as well as couplon activity, during MI in enzymatically isolated adult rabbit ventricular myocytes. The results suggest molecular mechanisms by which MI could interfere with EC coupling. We anticipate that this information may provide a basis for more detailed studies on the molecular basis of the failure of couplons during MI.

MATERIALS AND METHODS

Preparation of isolated myocytes

We isolated ventricular myocytes from adult New Zealand White rabbits (2.0 to 3.0 kg) using collagenase/protease digestion as described previously

Submitted June 20, 2007, and accepted for publication October 29, 2007.

Chana Chantawansri and Nhi Huynh contributed equally to this work.

Address reprint requests to Joshua I. Goldhaber, E-mail: jgoldhaber@mednet.ucla.edu.

Editor: David A. Eisner.

0006-3495/08/03/1656/11 $2.00

doi: 10.1529/biophysj.107.114892

(8), and in accordance with the guidelines of the UCLA Office for Protection of Research Subjects. After isolation, we stored cells for up to 6 h at room temperature (21–23°C) in a modified Tyrode's solution, containing (in mmol/L): 136 NaCl, 5.4 KCl, 0.33 NaH_2PO_4, 10 HEPES, 1 $MgCl_2$, 1.8 $CaCl_2$, and 10 glucose, pH 7.4, with NaOH. We also used this solution for loading cells with fluo-3 AM (Molecular Probes/Invitrogen, Eugene, OR) as described below.

Single Ca^{2+} channel recordings

To record single Ca^{2+} channel activity, we used the cell-attached patch technique with a patch amplifier (Axopatch 200B; Molecular Devices, Sunnyvale, CA) and a data acquisition system (Digidata 1322A; Molecular Devices) controlled by software (pClamp9; Molecular Devices). We used a 10 kHz sampling rate and filtered at 2 kHz using a −3 db, four-pole Bessel filter. Patch electrodes were pulled from borosilicate glass (Cat. No. G150F-4; Warner Instruments, Hamden, CT) on a horizontal puller (model No. P-97; Sutter Instruments, Novato, CA). Sylgard 184 (Dow Corning, Midland, MI) was applied to electrode tips for noise reduction. Electrodes had a tip diameter of 1–1.5 μm and a resistance of 7–13 MΩ when filled with internal solution containing (in mmol/L): $BaCl_2$ 110, TEA-Cl 30, HEPES 10, Tetrodotoxin 0.05 (EMD Biosciences, San Diego, CA), and glibenclamide 100 μmol/L, pH 7.4 with TEA-OH. Ba^{2+} was used as the charge carrier in place of Ca^{2+}. Glibenclamide was included to prevent activation of the metabolically sensitive I_{KATP} during application of the metabolic inhibitors. The control bath solution contained (in mmol/L): K-Aspartate 110, KCl 30, HEPES 10 mM, Glucose 10 mM, pH 7.4. We analyzed single channel records using commercial software (Clampfit 9.2; Molecular Devices).

Action potential recordings

To record the AP in isolated myocytes during simultaneous imaging of intracellular Ca^{2+}, we used the current-clamp mode of the whole cell patch-clamp technique. We stimulated APs with 5 ms square-wave pulses using a patch amplifier (Axopatch 200A; Molecular Devices) and a data acquisition system (Digidata 1200; Molecular Devices) controlled by software (pClamp8; Molecular Devices). Patch electrodes had a tip diameter of 2–3 μM, and a resistance of 1–3 MΩ when filled with internal solution containing (in mmol/L): 110 KCl, 20 HEPES, 10 NaCl, 5 Na-pyruvate, 5 $MgCl_2$, 2 EGTA, 1 $CaCl_2$, 1 KH_2PO_4, 1 KADP, 0.05 cAMP, and 1 Fluo-3, pH 7.2 with KOH. Pyruvate, KH_2PO_4, $MgCl_2$, and KADP were included as metabolic substrates for oxidative phosphorylation and ATP generation, and have been shown to delay metabolic rundown of the myocyte as effectively as ATP (9). The bath solution was the modified Tyrode's described above and extracellular glucose was the substrate for glycolysis. We added FCCP (50 nmol/L) to the bath and replaced glucose with 2-DG (10 mmol/L) to achieve MI as described previously (2).

Live imaging confocal microscopy

We prelabeled myocytes for Ca^{2+} imaging by incubating them for 30 min at 22°C in Tyrode's containing the Ca^{2+} indicator fluo-3/AM (30 μmol/L) and 0.007% Pluronic. Incubation was followed by two 20 min washes in dye-free Tyrode's. In addition, the patch pipette solution included fluo-3 salt and EGTA/Ca^{2+} as described above to optimize Ca^{2+} spike imaging (10). We find that a combination of fluo-3/AM together with fluo-3 salt in the pipette provides superior image quality during high speed line scanning. The concentrations of fluo-3, EGTA, and $CaCl_2$ in the patch electrode solution were chosen to limit the diffusion distance of free Ca^{2+} so that localized Ca^{2+} release events could be imaged during APs without reducing extracellular Ca^{2+} or applying Ca^{2+} channel blockers while maintaining SR Ca^{2+} stores (10). It has been proposed by Zahradnikova et al. (11) that this procedure produces Ca^{2+} spikes, a measure of Ca^{2+} release flux, rather than Ca^{2+} sparks. Probenecid (58.4 μM) was added to the bath to reduce extrusion of fluo-3. We obtained fluorescence images using the ultra-rapid line scan mode (0.55 ms/line) of a laser scanning confocal microscopy system (Odyssey XL; Noran Instruments, Middleton, WI) attached to an inverted microscope (Axiovert TV100; Zeiss, Jena, Germany) fitted with a 40× water immersion objective lens (C-Apochromat, 40/1.2 W Corr; Zeiss). Image acquisition was synchronized to APs using the digital outputs of the computer interface (Digidata, Molecular Devices) and the trigger input of the confocal system (Noran Instruments). Each image was preceded by a train of six conditioning APs at 0.5 Hz. The excitation wavelength of the Argon-Krypton laser was set to 488 nm, and fluorescence emission >510 nm was collected for image reconstruction. Pixel resolution was 0.19 μm. Image acquisition was synchronized with AP stimulation using the confocal microscopy system's workstation (Indy; Silicon Graphics, Mountain View, CA) to trigger the patch-clamp computer via the Digidata inputs. To reduce photobleaching as well as phototoxicity to the cells, the laser was shuttered electronically and triggered to open only during the acquisition period.

Image analysis

We identified and characterized Ca^{2+} spikes using custom software programmed in IDL 6.1 (RSI, Boulder, CO) and based on a popular algorithm (12). Spike probability was determined by dividing the number of spikes elicited at any given time point by the number of activated spikes in the same cell under control conditions. This method assumes a control spike probability of 100% in rabbit (10). We defined spike latency as the time interval between the AP stimulus and the earliest point where fluorescence reached 10% above the average resting value. To account for the rising diastolic Ca^{2+} concentration during MI in our ratioed images, we employed the following expression to correct the fluorescence ratio ($F/F_{0\ \mathrm{corrected}}$):

$$F/F_{0\,\mathrm{corrected}} = (F/F_0) \times (F_{0\,\mathrm{MI}}/F_{0\,\mathrm{Control}}).$$

Here, (F/F_0) is the fluorescence of each pixel in an image ratioed against its resting value before depolarization. ($F_{0\ \mathrm{MI}}/F_{0\ \mathrm{Control}}$) is the spatially averaged resting fluorescence during MI ratioed against the resting fluorescence during control. The latter term serves as a correction factor for the rising resting Ca^{2+} during MI. We calculated spike amplitude by subtracting the resting $F/F_{0\ \mathrm{corrected}}$ from the peak $F/F_{0\ \mathrm{corrected}}$.

Statistical analysis

All values are presented as mean ± SE. Error bars in figures depict mean ± SE and are shown when larger than symbols. We used paired Student's *t*-test or ANOVA with Dunnett's test for multiple comparisons when assessing statistical significance (JMP 5.0.1a, SAS Institute, Cary, NC). To test statistical significance of single Ca^{2+} channel open-time distribution, we used a resampling or bootstrap approach (13). A P value <0.05 was considered statistically significant.

Reagents

All reagents were obtained from Sigma-Aldrich (St. Louis, MO) unless otherwise specified in the text.

RESULTS

Effect of metabolic inhibition on single LCC properties

We know from our prior work that I_{Ca} declines during MI (1, 2). It is therefore reasonable to hypothesize that unless the

conductance of LCCs declines, there must be a change in other single channel properties. These include open probability (P_o), null probability (P_{Null}, the chance that an opening will not occur over a specified interval), latency, and open-time distribution. Each of these will influence the number of LCCs in a couplon that can trigger Ca^{2+} release during MI. To examine this hypothesis, we measured single LCC activity in cell-attached patches with repetitive 100-ms clamp pulses from −50 to +10 mV, using Ba^{2+} as the charge carrier.

Under control conditions, LCC openings were frequent, and first openings occurred shortly after depolarization (Fig. 1). The average magnitude of the single channel Ba^{2+} current was 0.98 ± 0.04 pA and there was no reduction after 6.5 min of MI (0.98 ± 0.07 pA, $n = 6$ cells, P = NS). Thus, MI does not significantly affect channel conductance, suggesting that MI reduces macroscopic Ca^{2+} current by reducing the number of channels that actually open or by reducing their open times rather than by altering the magnitude of unitary currents.

To examine this question directly, we plotted histograms of P_o for bin widths of 2 ms as a function of time over the course of the 100-ms clamp depolarization (Fig. 2 *A*). The histograms show that MI significantly reduces P_o at all times during the clamp, and this reduction is more pronounced as MI proceeds. Likewise, P_{Null}, the probability of no openings occurring during the first 50 ms of the voltage clamp, increases significantly during MI (Fig. 2 *B*). We chose the 50-ms value because we observed Ca^{2+} spike latencies this long during our imaging experiments (see below). Since the spike latencies at +50 mV (i.e., near the peak of the action potential) were as long as 50 ms, the value of P_{Null} we have chosen for +10 mV is probably conservative. The increase in P_{Null} is consistent with the reduction in P_o since the chance of a channel opening during any interval has declined. This suggests that fewer channels are available to trigger a release event within a specified time during MI.

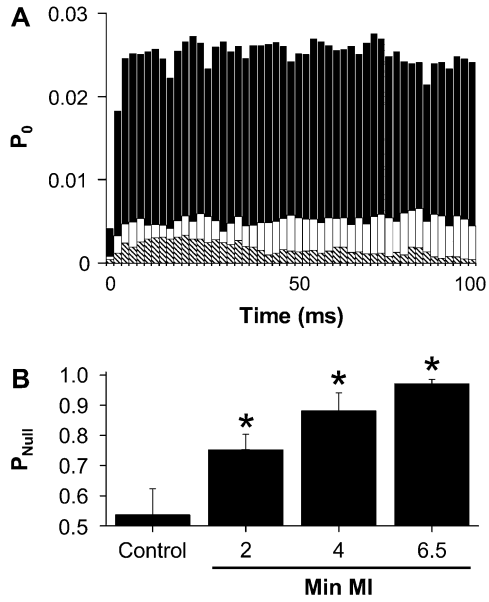

FIGURE 2 (*A*) Histograms of single Ca^{2+} channel open probability (P_o) at 2-ms bin-widths during 100-ms clamp depolarizations from −50 to +10 mV under three conditions: solid bars, control; open bars, 4 min MI; cross-hatched bars, 6.5 min MI. P_o is low for the first few ms of depolarization but rises quickly to a maximum by ~20 ms ($n = 6$ cells); (*B*) Bar graphs showing the increasing mean ± SE of the null probability (P_{Null}, the probability of no openings occurring during the first 50 ms of the voltage clamp) from six cells as MI progresses. *$p < 0.05$.

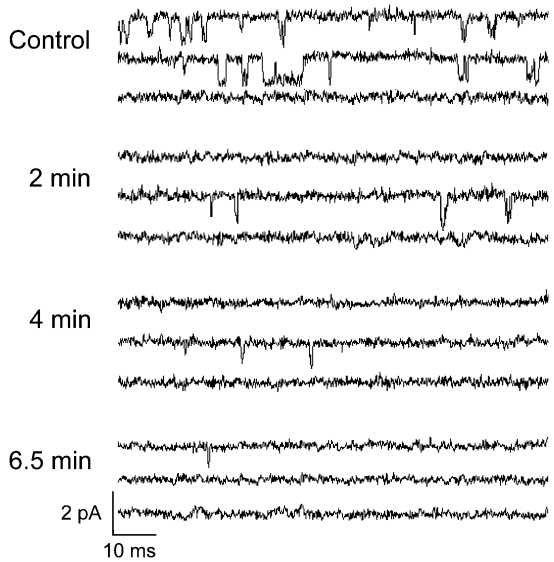

FIGURE 1 Cell-attached patch recordings of unitary Ba^{2+} currents through L-type Ca^{2+} channels in response to 100-ms voltage-clamps from −50 to +10 mV. Traces shown under control conditions and at 2, 4, and 6.5 min of MI. See text for details.

If the first latency of LCCs were significantly increased, this would have the effect of increasing P_{Null} and reducing the number of functioning channels during the interval when triggering occurs. We therefore examined the latency distribution of Ca^{2+} channels under control conditions and again after MI. Under control conditions, channel opening displayed a modal first-latency distribution (Fig. 3 *A*) typical of L-type Ca^{2+} current. Since we saw no evidence of amplitude multiples we assumed this distribution was based on single channel openings. Cavalie et al. (14) have pointed out that the distinct rising phase in the first latency distribution indicates a more complex reaction scheme than a simple first-order transition from a closed to an open state. This complexity is maintained during MI. All latency distributions can be described by an equation of the form $Y = A_1 \exp(-t/\tau_1) + A_2 \exp(-t/\tau_2)$. This equation was plotted in a normalized form, which clearly displays the modal nature of the first-latency distribution and reveals that the decay of this distribution is prolonged with progressive MI (Fig. 3 *B*). Thus with progressive MI, channel openings are less frequent while both the rising phase and the exponential decay

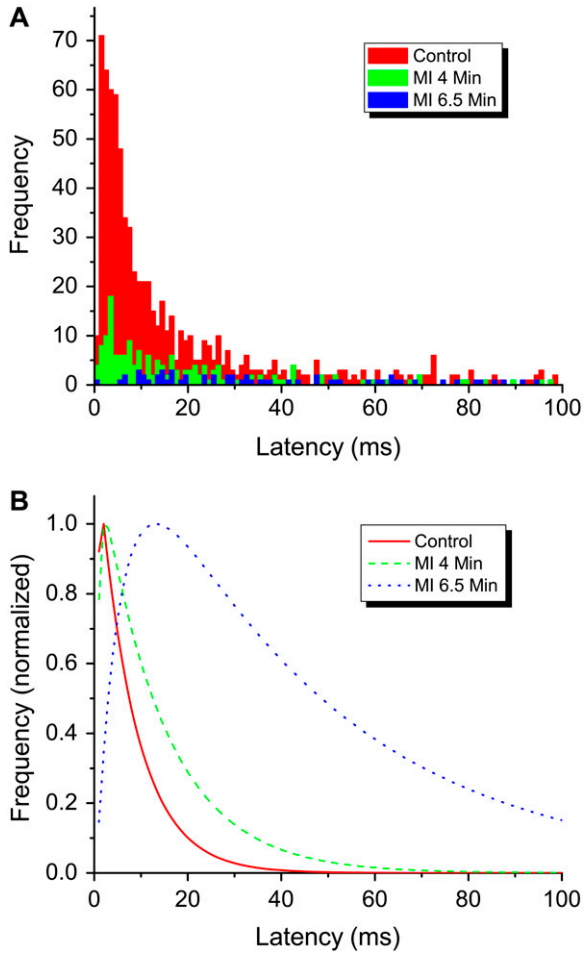

FIGURE 3 (*A*) Frequency distribution of single Ca^{2+} channel latencies during 1000 depolarizations from a representative cell under control conditions (*red*), and at 4 (*green*) and 6.5 (*blue*) min after application of metabolic inhibitors. MI clearly reduces the number of latencies, but this reduction is particularly striking at short latencies. (*B*) Exponential curve fits of the frequency data shown in panel *A*, plotted in normalized form. Note the modal nature of the fits under all conditions and the slowed rising and decay phases with progressive MI.

phase are slowed. Longer latencies, for example, >40 ms, are relatively more frequent in channels treated with metabolic inhibitors. To summarize, MI has the effect of significantly increasing first latency and will therefore delay the activation of I_{Ca}.

Open time distributions

After establishing that LCC openings are less frequent and delayed in onset during MI, we investigated the effect of MI on the distribution of LCC open times. These were plotted as open-time frequency histograms and were well fit by mono-exponential decays before and during MI (Fig. 4, *A* and *B*). Traditionally, two histograms are compared using statistics such as χ^2 or Kolmogorov-Smirnov. These tests, however, have a number of drawbacks. First, the χ^2 test is an approximation to an approximation, derived by Sir Ronald Fisher to make hand calculation easier (15). Second, there are many distributional assumptions underlying the derivation of the χ^2 formula, which may well not be satisfied by our distributions. Third, we are comparing histograms with a large number of elements (the control condition) to histograms with much smaller numbers (during MI). This creates problems for the application of both methods. Fourth, we specifically wanted information on where the two histograms differed. But both χ^2 and Kolmogorov-Smirnov analyses are designed to answer the simpler question, whether two distributions differ overall, and do not provide information on where they differ.

To address these concerns we used a resampling or bootstrap approach (13), which does not have these drawbacks. We designed the approach to test whether there is a statistically significant loss of longer open times during MI compared to shorter open times. We used the control data as our box model and then sampled from that box the same number of observations as were made during MI. This sample was binned using the same bins as the control and MI histograms and the histograms were then stored. This procedure was repeated 5000 times for each case. Then, for each bin, a 95% confidence interval was calculated around the actual counts in the control condition. If the bin count observed in the experimental condition lies above (or below) the 95% confidence band anywhere, we can say that the experimentally observed bin statistically has too many (or too few) entries compared to control.

Fig. 4 *C* illustrates this bootstrap analysis of the frequency distribution of single Ca^{2+} channel open-times from a representative cell exposed to metabolic inhibitors for 4 min. The solid line is the actual histogram showing the distribution of single channel open-times after MI. The shaded areas in each bin represent the 95% confidence band calculated by resampling the control histogram. Note that after MI, there is a significant excess of short open times compared to control, and a significant deficit of long open times. We obtained the same result in five of six cells treated with metabolic inhibitors.

Thus, MI reduces P_o and open-time, increases P_{Null}, and delays channel activation. These effects have predictable consequences for couplon activity, including a reduction in triggering, increased latency of triggering, and a resulting reduction and slowing of the Ca^{2+} transient during MI.

Effect of early metabolic inhibition on action potentials and evoked calcium spikes

Using ultra-rapid line scan confocal microscopy, we recorded Ca^{2+} spikes and spatially averaged Ca^{2+} release flux transients (fluo-3 fluorescence) evoked by APs under control conditions and at 1-min intervals after application of the metabolic inhibitors FCCP and 2-DG. Control APs display a rapid upstroke and early rapid transient repolarization,

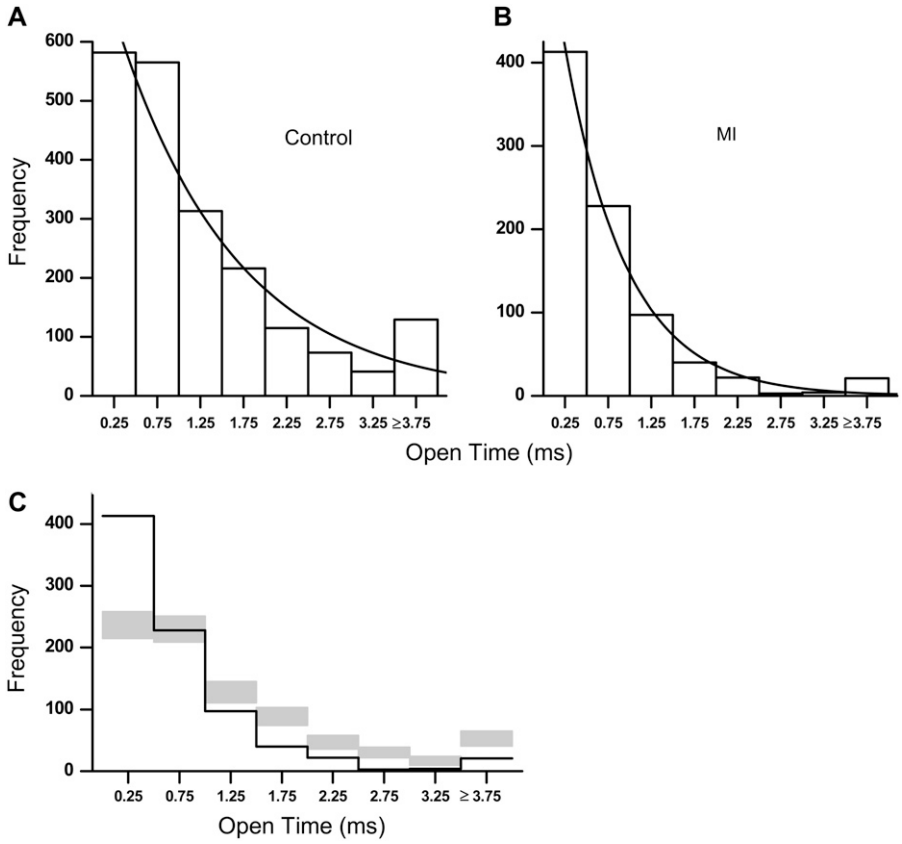

FIGURE 4 Single L-type Ca^{2+} channel open-time frequency histograms from a representative cell under control conditions (*A*) and during MI (*B*). We set our minimum detectable open time to 150 μs. A monoexponential fit is superimposed on the data. The fit did not include the 8th bin, i.e., open times $\geq$ 3.75 ms. Note the accelerated rate of decay of open-time frequencies and the corresponding disproportionate loss of long open times during MI. The bootstrap analysis of the change in the frequency distribution of open times during MI is shown in panel *C*. The shaded areas in each bin represent the 95% confidence band of the control data calculated by resampling. The solid line shows the actual values of the bins during MI. Note that there is an excess of short values during MI and a deficit of long values during MI compared to the resampled control data. Since the actual values lie outside the confidence band, we can conclude that there is a significant ($p < 0.05$) difference between control and MI.

followed by a plateau and slow repolarization typical of rabbit (Fig. 5). Spatially averaged Ca^{2+} release flux transients rise rapidly with a short time to peak and a steady decay.

During MI, AP duration shortens, though the extent and time course vary from cell to cell. Since changes in AP duration at 90% repolarization (APD_{90}) during MI reflect activation of the metabolically sensitive K^+ current I_{KATP} (16), we used APD_{90} as an index of the extent of MI in each cell. We can clearly discern shortening of the APD_{90} to ~75% of control after only 1 min of MI in the example displayed in Fig. 5. Shortening of the APD_{90} in response to MI has been described previously and is consistent with reduction of I_{Ca} and activation of I_{KATP} (1). After 6 min, the APD_{90} has declined to 50% of control. AP shortening at 6 min is associated with a decline in both the upstroke velocity and amplitude of the spatially averaged Ca^{2+} release flux transient, as we have described previously. Close examination of the images at 6 min in Figs. 5 and 6 shows a clear reduction in spike probability. We have shown previously that reduction in the number of active Ca^{2+} release sites fractionates the Ca^{2+} release pattern and is responsible for the reduction in the spatially averaged Ca^{2+} release flux transient (1,2). Spike amplitude remains unchanged during early MI, indicating that the flux of Ca^{2+} through those couplons that remain functioning does not change (17). This in turn implies preserved SR Ca^{2+} stores and RyR conductance in those couplons that remain active at this stage of MI. The time-to-peak (TTP) of spikes also remains constant, suggesting that the kinetics of functioning RyRs are unaffected by MI severe enough to shorten the APD_{90} by 50% (however, spike amplitude does change during prolonged MI, as discussed below). Changes in spatially averaged Ca^{2+} release flux, Ca^{2+} spike probability, Ca^{2+} amplitude, and TTP relative to the reduction in APD_{90} during MI are summarized in Fig. 7 ($n = 21$ cells and 420 couplons).

We also observe an increase in diastolic Ca^{2+} during MI (Fig. 5, summarized in Fig. 7), as described by others (18,19). This is caused by inhibition of mechanisms that extrude or take up Ca^{2+} from the cytosol (20). However, this does not necessarily lead to a reduction in SR Ca^{2+} content because the number of spikes, and therefore couplons, that are activated declines. Thus the extent of triggered Ca^{2+} release is also less. We and others have repeatedly shown that SR Ca^{2+} stores remain intact during MI (1,2,6,21).

Spike latencies during metabolic inhibition

The ultra-rapid line-scan technique affords us with a unique opportunity to examine the kinetic properties of Ca^{2+} spikes. Under control conditions, Ca^{2+} spikes exhibit short latencies (Fig. 6) and their activation is highly synchronized, i.e., the

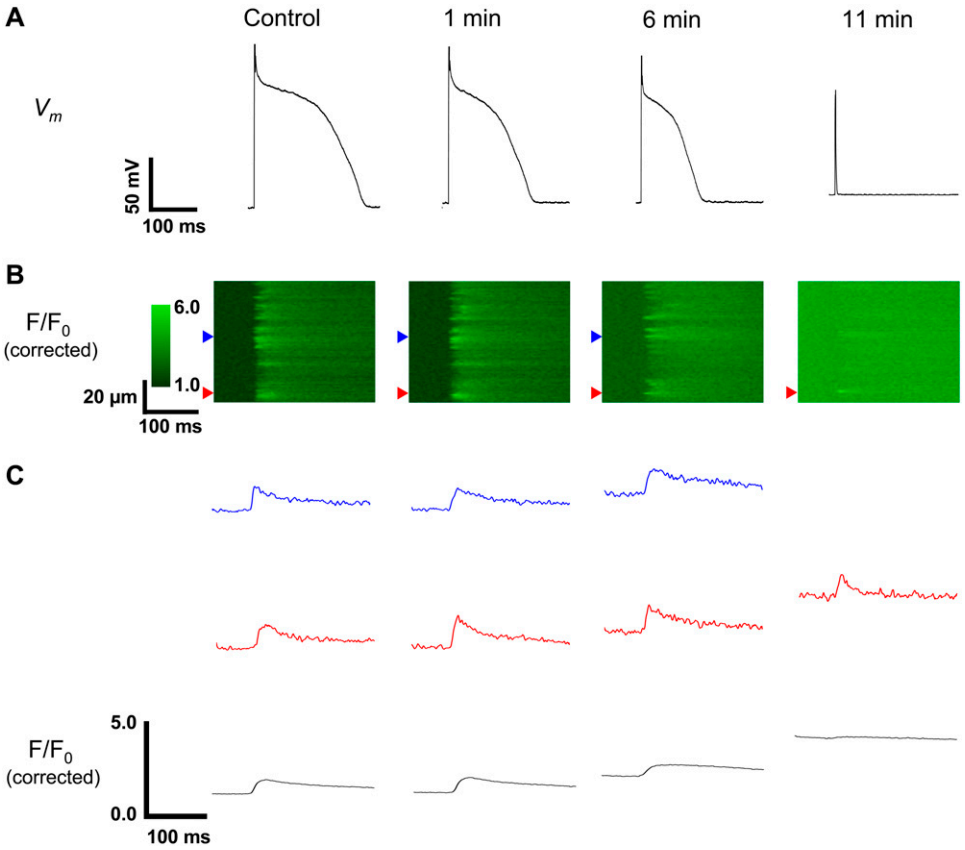

FIGURE 5 Action potentials (*A*) and simultaneously recorded high speed (0.55 ms/line) confocal images of Ca^{2+} spikes (*B*) under control conditions and during MI at 1, 6, and 11 min in a representative patch-clamped rabbit ventricular myocyte loaded with 1 mM fluo-3 and 2 mM EGTA. Linescan images were normalized to resting fluorescence (F/F_0) and then corrected for the rise in resting diastolic Ca^{2+} during MI (F/F_0 corrected). Blue and red arrows indicate locations of two different Ca^{2+} spikes along the scan line whose individual fluorescence profiles are shown in panel *C* for each time point during MI. The profile color matches the corresponding arrow. The bottom traces are the spatially averaged fluorescence transients taken from the images. We show these to emphasize both the rise in background Ca^{2+} and the decrease in the amplitude of the spatially averaged Ca^{2+} release flux transient during MI.

latency variance is small (see control histogram in Fig. 8). This occurs because the presence of numerous LCCs in a couplon increases the chance that at least one LCC will open with a short first latency, thereby triggering a spike with a short latency (5).

After 6 min of MI (when the APD_{90} is roughly 50% of control and spike release probability is reduced to ~70% of control), there is an increase in average spike latency (see, for example, the 6-min panel in Fig. 6) from 9.4 ± 0.5 to 15.0 ± 2.0 ms ($n = 21$ cells). Spike latency variance also increases as

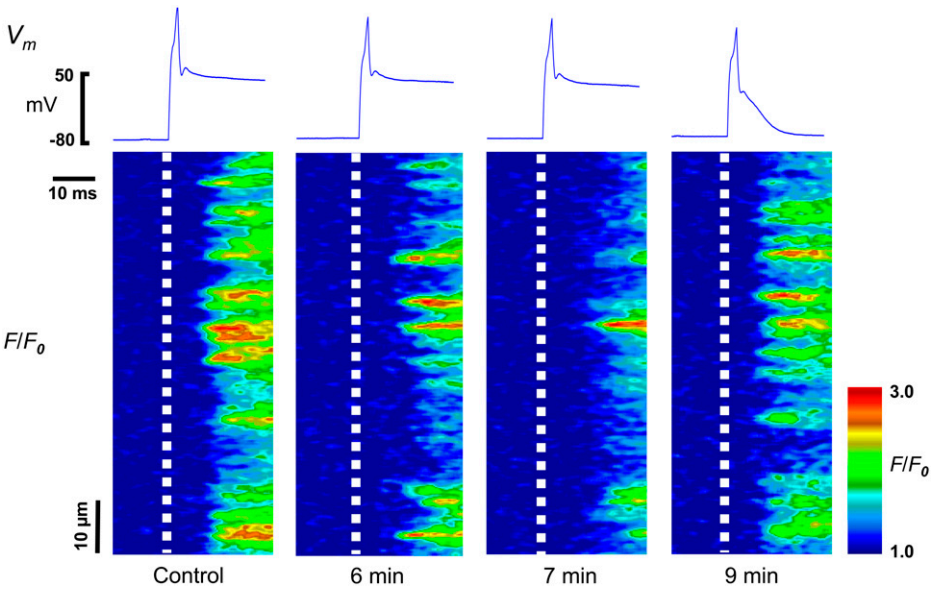

FIGURE 6 First 50 ms of action potentials (APs, *top row*) and corresponding normalized high-speed (0.55 ms/line) linescan images (F/F_0, *bottom row*) under control conditions and at 6, 7, and 9 min during MI in a representative rabbit myocyte. Timescales are matched to highlight the latency and frequency of spike onset after the upstroke of the AP. Dashed lines in the linescan images correspond to the AP stimulus. Note that spike occurrence is reduced and latency increased by 6 min and is even more pronounced at 7 min. In this example, the shorter AP at 9 min restores spike frequency to control levels and activates spikes with short latency and high synchrony (low variance). A stimulus artifact could not be separated from the upstroke of the AP.

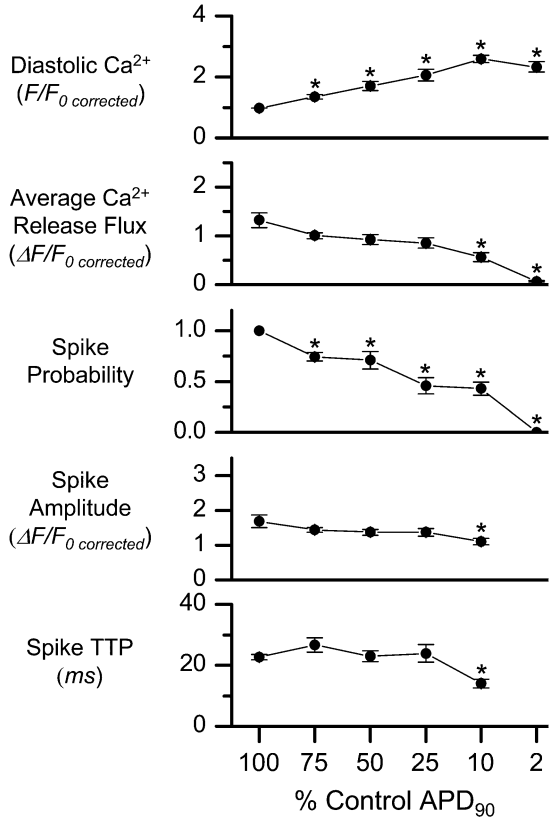

FIGURE 7 Summary data from 21 cells and 442 couplons showing the dependence of diastolic Ca^{2+} (F/F_0 corrected), the spatially averaged Ca^{2+} release flux ($\Delta F/F_0$ corrected), spike probability, spike amplitude ($\Delta F/F_0$ corrected), and spike time to peak (TTP, ms), on action potential duration relative to control (% Control APD_{90}; Control $APD_{90} = 100\%$) during MI. The position of the scan line was fixed to one location at all times during the protocol. $*p < 0.05$ by one-way ANOVA and Dunnett's test for multiple comparisons of mean cell values. Error bars for mean ± SE are shown only if larger than symbols.

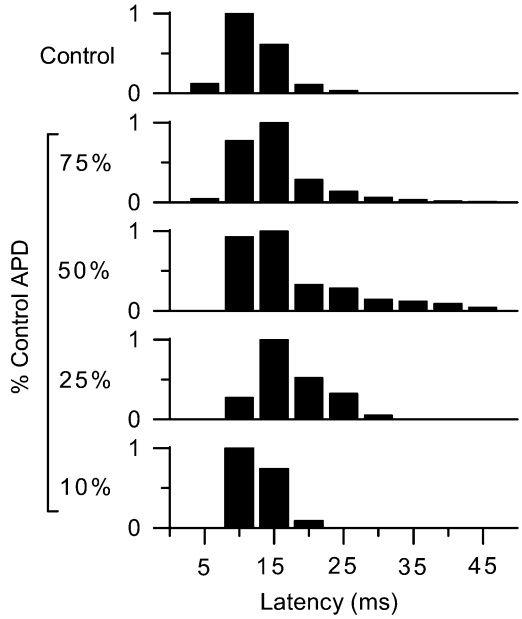

FIGURE 8 Normalized frequency histograms of spike latency (ms) under control conditions, and as the APD_{90} shortened during MI for 21 cells. Note the widened distribution of latencies as the APD_{90} shortened to 50% of control APD_{90} during MI and the subsequent narrowing of spike latencies as the AP became very short (10%). See text for explanation.

MI progresses, as shown in the histograms plotted in Fig. 8. Under control conditions, spike latencies are short and have a narrow distribution. The latest spikes occur 25 ms after the upstroke of the AP. When MI reduces the AP to 50% of control, latencies are distributed much more widely (see Fig. 8, 50%), with some spikes occurring as late as 40–50 ms after the upstroke of the AP when the membrane is still depolarized (close to +40 mV). This loss of synchronous spike onset is consistent with our observations on the effect of MI on LCC activity, in particular the increase in LCC latency and P_{Null} (taken at 50 ms as noted earlier) and the decline in LCC P_o.

Effect of more severe AP shortening (APD_{90} 10–25% of control)

Continued shortening of the APD_{90} to the 10–25% range during MI is associated with a further decline in spike probability (Fig. 7), which is not surprising considering that LCCs become inactive and are effectively lost with prolonged MI. But in contrast to the more modest reductions in AP duration described above, these much shorter APs (10–25% of control) are associated with reduced spike latency and variance. This finding is summarized in Fig. 8; the histograms at 25% and 10% of control APD_{90} show that the latency dispersion is reduced considerably when compared to less severe AP shortening. When the APD_{90} has declined to 10% of its control value, the distribution of spike latencies comes to resemble the control distribution, although it is less dispersed (Fig. 8). We also find that spike amplitude and TTP, previously unaffected by MI, have declined at this point. Since spike amplitude is a measure of Ca^{2+} flux through RyRs, and TTP of spikes a measure of RyR kinetics, these data suggest that inhibition of RyR activity begins during this late stage of MI.

In some cases during MI, almost all spikes are completely lost at APD_{90} 25%. However, in two interesting cases, further reduction of the APD resulted in restoration of Ca^{2+} spike activity (compare Fig. 6, at 7 min, where spikes are rare and at 9 min, where spikes recover; note that these two cells are included in the data presented in Figs. 7 and 8). We do not know why only two cells recovered in this fashion, as we were unable to identify any specific differences between these and other cells that did not exhibit recovery. They appear to be rare instances of cells that reside close to the threshold for inhibition. However, we note that the short AP at 9 min in Fig. 6 has a very rapid rate of repolarization and that the onset of recovered spikes begins when the membrane potential crosses 0 mV as it is repolarizing. This suggests that

an enlarged trigger, i.e., an early repolarization, is very likely contributing to the activation of spikes. Both Zahradnikova et al. (22) and Sah et al. (23) have shown that this pattern of membrane depolarization followed closely by repolarization is associated with increased EC coupling gain. This is in contrast to spikes evoked at earlier times during MI, which do not seem to be associated with significant membrane repolarization. Thus, although MI may have reduced the number of functioning LCCs and their open time, their ability to trigger has increased. As the APD_{90} becomes extremely short ($<2\%$), spikes are always abolished (Fig. 7), presumably because LCC activity is virtually abolished.

Two conclusions seem possible here. First, despite prolonged MI there are instances when RyRs can still be activated. Presumably an enlarged trigger can overcome inhibitory effects of MI on RyRs (1). The second conclusion is that, in those cases where short APs reactivate spikes despite prolonged MI, there must remain a significant number of functioning LCCs because triggering is clearly restored (see Discussion for an estimate of the number).

DISCUSSION

Metabolic inhibitors reduce the activity of both LCCs and RyRs (1,2,6). Thus, we expect any loss of Ca^{2+} spikes and reduction in the Ca^{2+} transient during MI to proceed from these. However, the extent to which spikes fail as a result of one cause versus the other is unknown. Both LCC and spike characteristics such as probability, latency, and variance can provide valuable insight into the mechanism of EC coupling failure during MI, as well as fundamental insight into couplon structure.

Effects of metabolic inhibition on LCCs

MI reduces I_{Ca} in patch-clamped guinea pig (1) and rat ventricular myocytes (2). This study is, to our knowledge, the first to demonstrate the single channel basis for this decrease in I_{Ca} and the resultant effects on Ca^{2+} spike activation during MI. I_{Ca} could fail during MI either because the magnitude of the unitary current declines or because some process associated with the activation of I_{Ca} is impaired so that channel openings are less frequent or of shorter duration. Our results suggest that channel conductance is not affected by MI. Thus spike failure is not a consequence of trigger failure caused by the decline in the magnitude of unitary currents. For this reason we analyzed various parameters associated with LCC activation.

The first latency of LCCs showed a striking prolongation during MI (Fig. 3). Thus one can see that after 4 min of MI the frequency of first latencies at 4 ms (peak value of control) fell to $\sim$10% of control. If we assume a similar relative change in first latency at +50 mV when Ca^{2+} is the charge carrier, it is apparent that part of the explanation for the increase in Ca^{2+} spike latency would simply be a reduction in the chance that a spike will be triggered by an LCC within the first few milliseconds of membrane depolarization (24). The decline in P_o and the increase in P_{Null} with MI are also expected to reduce I_{Ca} as well as the chance that spikes will be triggered. Finally, reduced open times are expected to reduce spike probability simply because the likelihood that a spike is triggered will depend on the integral of Ca^{2+} flux through a channel opening (25). This flux is reduced when the open time is reduced.

We cannot exclude the possibility that increases in cytoplasmic Ca^{2+} during MI (e.g., Fig. 5) may be inactivating LCCs. Reductions in pH (26) or changes in phosphorylation state could also have considerable influence on LCC activation during MI. A large increase in proton concentration is a well-known consequence of sodium-hydrogen exchange blockade, which is caused by ischemia and hypoxia (27,28). However, since we do not know the extent of acidification under our experimental conditions, further speculation is unwarranted. Some of the effects of MI on LCCs are consistent with the known effects of CaMKII on these channels (29,30). It appears that CaMKII colocalizes at dyads (31). If the CaMKII that is responsible for phosphorylating LCCs is associated with a glycolytic complex, as it is in the SR (32), we speculate that substances such as 2-DG, which block glycolytic production of ATP, would reduce CaMKII phosphorylation of LCCs. Thus, we consider the inference that MI might exert some, if not all, of its effects on LCCs via CaMKII to be reasonable.

Our single channel results were obtained in 110 mmol/L Ba^{2+} at +10 mV. Charge screening at this high concentration of Ba^{2+} would be expected to shift the voltage-dependence of the channels by ~ -30 mV (33). Therefore, the results obtained at a test potential of +10 mV should correspond to ~ -20 mV at a physiological concentration of divalent ions. We see no a priori reason for assuming that at least qualitatively the effect of MI on LCC activation when the channels conduct Ba^{2+} would be significantly different from its effect on these channels when they conduct Ca^{2+}.

Effects of metabolic inhibition on spike probability and latency

As mentioned in the previous section, several effects of MI on spikes can be explained by changes in the characteristics of the LCCs that trigger them. The increase in LCC latency and the decline in LCC open probability are sufficient to account for the increase in spike latency and the decline in spike probability that are apparent when the APD_{90} reaches 50% of control (Figs. 7 and 8). This is compounded by the increase in LCC null probability, which means that in effect functioning LCCs cease to exist. With fewer active LCCs, the chances of a channel opening with a short latency decrease. Finally, because LCC open times shorten during MI, those open times which are already short may cease to transmit enough calcium to trigger spikes, regardless of

whether the RyR function is deficient or not. It is worth emphasizing that until the AP becomes short (<50%), the effect of MI on spikes qualitatively reflects the effect of MI on first latency of LCCs. However, as we shall discuss in a moment, this simple relationship is confounded when the AP becomes shorter.

The decrease in spike latency that occurs during the continued decline in spike probability has a slightly more complicated explanation. Zahradnikova et al. (22) have shown that short depolarization followed by repolarization (and we consider short APs to be similar to the short depolarizations they described) can increase the gain of EC coupling. We propose that when APs become short during MI, they repolarize during very short LCC openings that cannot normally trigger. However, since repolarization takes place when LCCs are still open (e.g., Fig. 6; 9 min), a larger amount of calcium is transmitted through them because Ca^{2+} is subject to a greater inward electrochemical potential when the cell has repolarized. Thus LCCs again become capable of triggering, i.e., the system acquires the high gain suggested by Zahradnikova et al. (22). Deactivation of any open channels will occur when the short AP repolarizes, imposing a reduced latency on the population of remaining available channels. Thus triggered spikes during short APs will have a reduced probability, and a short latency.

Thus, we can explain the loss of spikes during MI without requiring compromised RyR activity. On the other hand, if RyR activity is deficient, the increased flux due to early repolarization could overcome their inhibition. Interestingly, Xu et al. (7) found that increased Ca^{2+} can gate RyRs suppressed by reduced pH. It is only after very prolonged MI that adverse effects on RyRs become apparent, and we shall discuss this in the next section.

Effect of metabolic inhibition on spike amplitude and the inhibition of RyRs

Arguments in the preceding sections suggest that the effects of MI on LCCs are sufficient to explain the changes that occur in spike characteristics until the advanced stages of MI when the APD_{90} becomes very short, e.g., 10% or less. At that advanced stage of MI, spike amplitude and TTP have clearly declined. It is well known that RyRs are sensitive to metabolic stress (1,2,6). Whether this is simply a consequence of reduced cellular ATP levels, increased ADP levels, reductions in pH, altered NADH levels, or increases in free Mg^{2+} is unknown, but all of these may contribute to RyR suppression (6,7,34–38). We estimate that FCCP and 2-DG reduced ATP in our cells to ~100–300 μmol/L, well above the concentration (10–50 μmol/L) associated with cellular rigor (39), but sufficiently low in the presence of ADP to activate I_{KATP} and shorten the AP (16). We do not think there are major changes in pH and Mg^{2+}, which if present would confound interpretation of results. Reductions in pH are probably limited by the buffering capacity of the patch electrode solution and lack of diffusion barriers in a single cell (1). To avoid significant increases in free Mg^{2+} caused by MI-induced reductions in ATP and increases in Ca^{2+} and ADP, we included 5 mM Mg^{2+} along with 1 mM ADP and 2 mM EGTA in the pipette solution. Even if free Ca^{2+} during a spike rises to 1 μmol/L, free Mg^{2+} will be maintained close to 4 mmol/L under these ionic conditions (as calculated by WEBMAXC (40)). It is therefore unlikely that MI will further increase the effect of Mg^{2+} on RyR and LCC function since it is probably already saturated.

The reduced spike amplitude indicates a reduction in couplon Ca^{2+} release flux. We can express the flux of Ca^{2+} through a cluster of RyRs in a couplon as $J_{RyR} = NP_oP_{RyR} \times [Ca^{2+}]_{SR}$, where N is the number of RyRs in the cluster, P_o the open probability of RyRs in the cluster, P_{RyR} the permeability of RyRs, and $[Ca^{2+}]_{SR}$ the concentration of Ca^{2+} in the SR. This relationship assumes that no membrane potential exists across the SR membrane and that cytosolic Ca^{2+} is sufficiently low that it does not greatly affect the initial release flux. If MI were to significantly affect RyRs we might expect it to reduce either RyR P_o or P_{RYR}. At least in the case of LCCs, their conductance does not appear to be affected by MI and we assume that the same holds true for RyRs. If P_o were to decline with MI we would expect a progressive decline in J_{RyR} and hence a decline in spike amplitude, unless there was a simultaneous increase in luminal Ca^{2+}, which does not appear to be the case (1,2); however, see Overend et al. (6). Thus we would expect to see a decline in spike amplitude with progressive MI if P_o were affected. We cannot demonstrate a statistically significant decline in spike amplitude until APD_{90} reaches 10% of control (Fig. 7), consistent with a reduction in the open probability for RyRs. The abbreviated TTP at 10% APD is consistent with this reduction in spike amplitude. However, the decline in amplitude, while statistically significant, appears to be small and we suggest that the main effect of MI on spike properties is attributable to its effect on LCCs discussed earlier. It is also likely that in cases where spikes reappear after prolonged MI and the AP is extremely short, the increased flux of Ca^{2+} through LCCs should to some extent overcome any inhibitory effect of MI on RyRs. Thus increased flux of Ca^{2+} through LCCs could mask the effect of MI on RyRs. Unfortunately, we cannot unambiguously separate the effects of MI on LCCs and RyRs.

Implications for couplon structure and function

Clusters of LCCs trigger Ca^{2+} sparks and spikes (10,11). Couplons containing large clusters of LCCs (large couplons) are associated with high spike probability and short spike latency (5). This is simply because the larger the cluster, the greater the chances of an LCC opening with both a short first latency and also an adequate open time to trigger a spike. Smaller clusters (associated with smaller couplons) are more likely to be associated with lower spike probability and

longer spike latencies. Although the exact mechanism for reduction in LCC open probability during MI is uncertain, the net effect is to reduce the number of functional LCCs in a couplon. If we assume that couplon sizes are distributed homogeneously, MI will reduce the average size of a couplon (by reducing the number of functioning LCCs in each couplon). Small couplons may be completely lost while large couplons will become smaller. This will have the net effect of both reducing spike probability and also increasing spike latency (because the chances of finding an LCC opening with a short latency are diminished). In addition, the variance of spike latencies increases with MI and therefore spikes become less synchronized. The increase in variance can be explained as follows: if we make the simplifying assumption that spike latencies are distributed according to a simple exponential decay, then the variance of the latencies will be equal to the mean of the distribution, which will also equal τ, the time constant of decay. If, as it appears in Fig. 8, τ increases during MI, then spike variance will also increase. We should also make it clear that an increase in τ, and therefore spike variance, could proceed either from a loss of triggering LCCs or alternatively a change in LCC latency distribution without necessarily losing triggering LCCs. As we have already indicated, when the AP becomes very short, factors that reduce τ begin to affect the variance of spikes, which become more synchronized.

Even though the number of LCCs that function may be reduced by MI, the fact that very short APs trigger with high fidelity suggests that the number of LCCs in a couplon could be large. So far as we are aware, this effect of MI has not been described before. If we assume that there is a significant flux of Ca^{2+} through first openings of available LCCs, we can use the equation $P_S = 1-(P_{Null})^N$, where P_S is the spike probability, to approximate N, the number of available channels in a couplon (10). 1-P_{Null} is quite simply the chance that at least one LCC will open if there is one channel available to open. If there are N channels in the couplon, then $1-(P_{Null})^N$ is the chance that there will be at least one opening, although there could be many channels available to open. With the simplifying assumption that the first opening triggers, we now make a quantitative speculation designed to illustrate that the number of LCCs in a couplon could in fact be quite large. If after 9 min of MI spikes reappear at a P_S of 0.8 (consistent with our data in Fig. 6) and P_{Null} is 0.95 (consistent with our data in Fig. 2), then we can calculate that $N = 32$. The assumption that a first opening can trigger is made plausible by the fact that during very short APs, Ca^{2+} flux through LCCs will be increased because of the increased driving force during rapid repolarization. Although we have stated that P_{Null} could be 0.95, this is based on measurements in Ba^{2+} at +10 mV. Under the physiological circumstances of this experiment, when spikes are restored, P_{Null} might actually be different and if it were lower, would reduce our estimate of N, particularly if our assumption that the first opening triggers is not correct.

In conclusion, to explain the effects of MI on spike genesis in rabbit ventricular cells, it is necessary to postulate that although a single LCC may trigger a spike, (and quite possibly the first opening of an LCC may trigger a spike) there are very likely to be clusters of LCCs in a couplon. If only one LCC triggered, we would not regard the remaining LCCs in a cluster as redundant since they ensure an increased probability of spike triggering (10). One might be inclined to think that all these results could be explained if there are not clusters of LCCs and a single LCC is responsible for triggering a spike. Increases in the latency of a couplon composed of a single LCC with MI would certainly prolong spike latency and increase its variance. However, it is extremely difficult to see how spikes with short latencies could be restored by short APs if this were the case.

The authors acknowledge the technical assistance of T. K. Duong, D. Philipson, and S. Zhang, and helpful comments by Dr. Alexey Zaitsev and Dr. Leighton Izu.

This work was supported by National Institutes of Health R01 No. HL70828 and the Laubisch Endowment for Cardiovascular Research.

REFERENCES

1. Goldhaber, J. I., J. M. Parker, and J. N. Weiss. 1991. Mechanisms of excitation-contraction coupling failure during metabolic inhibition in guinea-pig ventricular myocytes. *J. Physiol.* 443:371–386.
2. Fukumoto, G. H., S. T. Lamp, C. Motter, J. H. Bridge, A. Garfinkel, and J. I. Goldhaber. 2005. Metabolic inhibition alters subcellular calcium release patterns in rat ventricular myocytes: implications for defective excitation-contraction coupling during cardiac ischemia and failure. *Circ. Res.* 96:551–557.
3. Stern, M. D. 1992. Theory of excitation-contraction coupling in cardiac muscle. *Biophys. J.* 63:497–517.
4. Franzini-Armstrong, C., F. Protasi, and V. Ramesh. 1999. Shape, size, and distribution of Ca^{2+} release units and couplons in skeletal and cardiac muscles. *Biophys. J.* 77:1528–1539.
5. Inoue, M., and J. H. Bridge. 2005. Variability in couplon size in rabbit ventricular myocytes. *Biophys. J.* 89:3102–3110.
6. Overend, C. L., D. A. Eisner, and S. C. O'Neill. 2001. Altered cardiac sarcoplasmic reticulum function of intact myocytes of rat ventricle during metabolic inhibition. *Circ. Res.* 88:181–187.
7. Xu, L., G. Mann, and G. Meissner. 1996. Regulation of cardiac Ca^{2+} release channel (ryanodine receptor) by Ca^{2+}, H^+, Mg^{2+}, and adenine nucleotides under normal and simulated ischemic conditions. *Circ. Res.* 79:1100–1109.
8. Goldhaber, J. I., L. H. Xie, T. Duong, C. Motter, K. Khuu, and J. N. Weiss. 2005. Action potential duration restitution and alternans in rabbit ventricular myocytes: the key role of intracellular calcium cycling. *Circ. Res.* 96:459–466.
9. Goldhaber, J. I., S. Ji, S. T. Lamp, and J. N. Weiss. 1989. Effects of exogenous free radicals on electromechanical function and metabolism in isolated rabbit and guinea pig ventricle: implications for ischemia and reperfusion injury. *J. Clin. Invest.* 83:1800–1809.
10. Inoue, M., and J. H. Bridge. 2003. Ca^{2+} sparks in rabbit ventricular myocytes evoked by action potentials: involvement of clusters of L-type Ca^{2+} channels. *Circ. Res.* 92:532–538.
11. Zahradnikova, A., Jr., E. Polakova, I. Zahradnik, and A. Zahradnikova. 2007. Kinetics of calcium spikes in rat cardiac myocytes. *J. Physiol.* 578:677–691.
12. Cheng, H., L. S. Song, N. Shirokova, A. González, E. G. Lakatta, E. Ríos, and M. D. Stern. 1999. Amplitude distribution of calcium sparks

in confocal images: theory and studies with an automatic detection method. *Biophys. J.* 76:606–617.

13. Efron, B., and R. Tibshirani. 1991. Statistical data analysis in the computer age. *Science.* 253:390–395.
14. Cavalie, A., R. Ochi, D. Pelzer, and W. Trautwein. 1983. Elementary currents through Ca^{2+} channels in guinea pig myocytes. *Pflugers Arch.* 398:284–297.
15. Freedman, D., R. Pisani, and R. Purves. 1988. Statistics, 3rd Ed. Norton, New York.
16. Zingman, L. V., A. E. Alekseev, D. M. Zingman-Hodgson, and A. Terzic. 2007. ATP-sensitive potassium channels: metabolic sensing and cardioprotection. *J. Appl. Physiol.* Epub ahead of print.
17. Song, L. S., J. S. Sham, M. D. Stern, E. G. Lakatta, and H. Cheng. 1998. Direct measurement of SR release flux by tracking ''Ca^{2+} spikes'' in rat cardiac myocytes. *J. Physiol.* 512:677–691.
18. Barry, W. H., G. A. Peeters, C. A. F. Rasmussen, Jr., and M. J. Cunningham. 1987. Role of changes in $[Ca^{2+}]_i$ in energy deprivation contracture. *Circ. Res.* 61:726–734.
19. Eisner, D. A., C. G. Nichols, S. C. O'Neill, G. L. Smith, and M. Valdeolmillos. 1989. The effects of metabolic inhibition on intracellular calcium and pH in isolated rat ventricular cells. *J. Physiol.* 411: 393–418.
20. Seki, S., and K. T. MacLeod. 1995. Effects of anoxia on intracellular Ca^{2+} and contraction in isolated guinea pig cardiac myocytes. *Am. J. Physiol.* 268:H1045–H1052.
21. Stern, M. D., H. S. Silverman, S. R. Houser, R. A. Josephson, M. C. Capogrossi, C. G. Nichols, J. W. Lederer, and E. G. Lakatta. 1988. Anoxic contractile failure in rat heart myocytes is caused by failure of intracellular calcium release due to alteration of the action potential. *Proc. Natl. Acad. Sci. USA.* 85:6954–6958.
22. Zahradnikova, A., Z. Kubalova, J. Pavelkova, S. Gyorke, and I. Zahradnik. 2004. Activation of calcium release assessed by calcium release-induced inactivation of calcium current in rat cardiac myocytes. *Am. J. Physiol.* 286:C330–C341.
23. Sah, R., R. J. Ramirez, and P. H. Backx. 2002. Modulation of Ca^{2+} release in cardiac myocytes by changes in repolarization rate: role of phase-1 action potential repolarization in excitation-contraction coupling. *Circ. Res.* 90:165–173.
24. Cheng, H., M. B. Cannell, and W. J. Lederer. 1994. Propagation of excitation-contraction coupling into ventricular myocytes. *Pflugers Arch.* 428:415–417.
25. Lamb, G. D., D. R. Laver, and D. G. Stephenson. 2000. Questions about adaptation in ryanodine receptors. *J. Gen. Physiol.* 116:883–890.
26. Irisawa, H., and R. Sato. 1986. Intra- and extracellular actions of proton on the calcium current of isolated guinea pig ventricular cells. *Circ. Res.* 59:348–355.
27. Murphy, E., M. Perlman, R. E. London, and C. Steenbergen. 1991. Amiloride delays the ischemia-induced rise in cytosolic free calcium. *Circ. Res.* 68:1250–1258.
28. Anderson, S. E., E. Murphy, C. Steenbergen, R. E. London, and P. M. Cala. 1990. Na-H exchange in myocardium: effects of hypoxia and acidification on Na and Ca. *Am. J. Physiol.* 259:C940–C948.
29. Wu, Y., I. Dzhura, R. J. Colbran, and M. E. Anderson. 2001. Calmodulin kinase and a calmodulin-binding ''IQ'' domain facilitate L-type Ca^{2+} current in rabbit ventricular myocytes by a common mechanism. *J. Physiol.* 535:679–687.
30. Dzhura, I., Y. Wu, R. J. Colbran, J. R. Balser, and M. E. Anderson. 2000. Calmodulin kinase determines calcium-dependent facilitation of L-type calcium channels. *Nat. Cell Biol.* 2:173–177.
31. Wu, Y., L. B. MacMillan, R. B. McNeill, R. J. Colbran, and M. E. Anderson. 1999. CaM kinase augments cardiac L-type Ca^{2+} current: a cellular mechanism for long Q-T arrhythmias. *Am. J. Physiol.* 276: H2168–H2178.
32. Singh, P., M. Salih, J. J. Leddy, and B. S. Tuana. 2004. The muscle-specific calmodulin-dependent protein kinase assembles with the glycolytic enzyme complex at the sarcoplasmic reticulum and modulates the activity of glyceraldehyde-3-phosphate dehydrogenase in a Ca^{2+}/calmodulin-dependent manner. *J. Biol. Chem.* 279:35176–35182.
33. McDonald, T. F., A. Cavalie, W. Trautwein, and D. Pelzer. 1986. Voltage-dependent properties of macroscopic and elementary calcium channel currents in guinea pig ventricular myocytes. *Pflugers Arch.* 406:437–448.
34. O'Neill, S. C., and D. A. Eisner. 2003. pH-dependent and -independent effects inhibit Ca^{2+}-induced Ca^{2+} release during metabolic blockade in rat ventricular myocytes. *J. Physiol.* 550:413–418.
35. Zima, A. V., J. A. Copello, and L. A. Blatter. 2004. Effects of cytosolic $NADH/NAD^+$ levels on sarcoplasmic reticulum Ca^{2+} release in permeabilized rat ventricular myocytes. *J. Physiol.* 555:727–741.
36. Meissner, G. 1994. Ryanodine receptor/Ca^{2+} release channels and their regulation by endogenous effectors. *Annu. Rev. Physiol.* 56:485–508.
37. Balnave, C. D., and R. D. Vaughan-Jones. 2000. Effect of intracellular pH on spontaneous Ca^{2+} sparks in rat ventricular myocytes. *J. Physiol.* 528:25–37.
38. Kermode, H., A. J. Williams, and R. Sitsapesan. 1998. The interactions of ATP, ADP, and inorganic phosphate with the sheep cardiac ryanodine receptor. *Biophys. J.* 74:1296–1304.
39. Nichols, C. G., and W. J. Lederer. 1990. The role of ATP in energy-deprivation contracture in unloaded rat ventricular myocytes. *Can. J. Physiol. Pharmacol.* 68:183–194.
40. Patton, C., S. Thompson, and D. Epel. 2004. Some precautions in using chelators to buffer metals in biological solutions. *Cell Calcium.* 35: 427–431.